A Numerical Study of Thermal Dispersion in Porous Media

F. Kuwahara

A. Nakayama

H. Koyama

Department of Mechanical Engineering,
Shizuoka University,
3-5-1 Johoku, Hamamatsu, 432 Japan

Thermal dispersion in convective flow in porous media has been numerically investigated using a two-dimensional periodic model of porous structure. A macroscopically uniform flow is assumed to pass through a collection of square rods placed regularly in an infinite space, where a macroscopically linear temperature gradient is imposed perpendicularly to the flow direction. Due to the periodicity of the model, only one structural unit is taken for a calculation domain to resolve an entire domain of porous medium. Continuity, Navier–Stokes and energy equations are solved numerically to describe the microscopic velocity and temperature fields at a pore scale. The numerical results thus obtained are integrated over a unit structure to evaluate the thermal dispersion and the molecular diffusion due to tortuosity. The resulting correlation for a high-Peclet-number range agrees well with available experimental data.

Introduction

The complexity associated with the geometric structure of a porous medium does not allow us to treat the detailed velocity and temperature fields inside each individual porous structure. Thus, it has been a common practice to introduce volume-averaged quantities and concentrate on the overall aspects of mass, momentum, and energy conservation principles (e.g., Quintard and Whitaker, 1993). Accordingly, a number of heuristic and semi-heuristic models have been introduced to describe Darcy and non-Darcy flows and dispersion in heat and mass transfer through a porous medium. The model constants in these models are usually determined on the basis of exhaustive experimental data.

Detailed flow and temperature fields inside a microscopic structure may be investigated using a periodic structure (such as lattice structures) rather than treating complex porous media in reality. Eidsath et al. (1983), Coulaud et al. (1988), Sahraoui and Kaviany (1991), and Fowler and Bejan (1994) carried out two-dimensional numerical simulations for flows across banks of circular cylinders, whereas the authors (Kuwahara et al., 1994; Nakayama et al., 1995) investigated a collection of square rods to cover a wide range of porosity, virtually from zero to unity. Three-dimensional analyses were also conducted by Larson and Higdon (1989) for Stokes flows through lattice of spheres, and by the authors (1995) for fully elliptic flows through a lattice of cubes to study not only the Darcy contribution but also the porous inertial contribution to the macroscopic pressure drop.

Dispersion in porous media was studied by Koch and Brady (1985) and Koch et al. (1989) who obtained closed-form expressions for the dispersion tensor. However, in their analysis, an extremely dilute suspension of particles (i.e., high porosity) having the same thermal conductivity as the fluid was assumed using Stokes flow approximation along with the point force approximation. Thus, no Reynolds number and boundary layer effects were implemented, and the transverse dispersion coefficient was found to be independent of Peclet number and less than the thermal diffusivity of fluid. Full Navier–Stokes and energy equations were solved by Eidsath et al. (1983) and Edwards et al. (1991) for flows through a periodic structure of circular cylinders with in-line and staggered arrangements. In their models, the thermal conductivity of particles is assumed to be zero, such that no coupling of the energy equations for the fluid and solid phases was present. Kuwahara et al. (1994) proposed an idea to determine the transverse dispersion coefficient by fitting the numerical results against the similarity solution for forced convection from a line heat source in a porous medium, and conducted exhaustive numerical calculations for a large computational domain made of lattice of square rods. Arquis et al. (1991, 1993) extended the numerical model proposed by Coulaud et al. (1988) to the coupling of momentum and heat transfer to study both axial and transverse dispersion coefficients. The elegance of the work by Arquis and his group is that they imposed a macroscopic temperature gradient either normal or parallel to a macroscopically uniform flow such that the microscopic temperature field within only one structural unit is needed, as in the velocity field, to determine the corresponding dispersion coefficient. However, in these numerical studies, computations were carried out only for a limited number of sets of the parameters such as the porosity, macroscopic flow direction, and Peclet number. No general functional relationships for the dispersion coefficient as a function of these parameters were drawn from these studies due to a rather narrow porosity range.

In the present study, we follow the numerical approach proposed by Arquis et al. to determine the transverse dispersion coefficient purely from a theoretical basis. A macroscopically uniform flow is assumed to pass through a lattice of square rods placed regularly in an infinite space, where a macroscopically linear temperature gradient is imposed perpendicularly to the flow direction. The macroscopic flow angle is varied every 5 deg to investigate geometric effects on the dispersion coefficient. The present numerical model made of a lattice of square rods allows us to change the porosity virtually from zero to unity, and to establish a possible correlation for the dispersion coefficient. We strictly follow the mathematical definition of dispersion correlation in an exact form, appearing in the volume-averaged energy equation, and isolate it from the tortuosity contribution. (Note that Arquis et al. did not treat these apparent conductivities individually.)

Numerical Model and Boundary Conditions

We shall consider a macroscopically uniform flow with an angle θ meandering through an infinite number of square rods placed in a regular fashion, where a macroscopically linear temperature gradient is imposed perpendicularly to the flow direction, as illustrated in Fig. 1. Thus, the macroscopic velocity and temperature fields follow:

Contributed by the Heat Transfer Division for publication in the JOURNAL OF HEAT TRANSFER. Manuscript received by the Heat Transfer Division October 9, 1995; revision received March 29, 1996. Keywords: Forced Convection, Numerical Methods, Porous Media. Associate Technical Editor: K. Vafai.

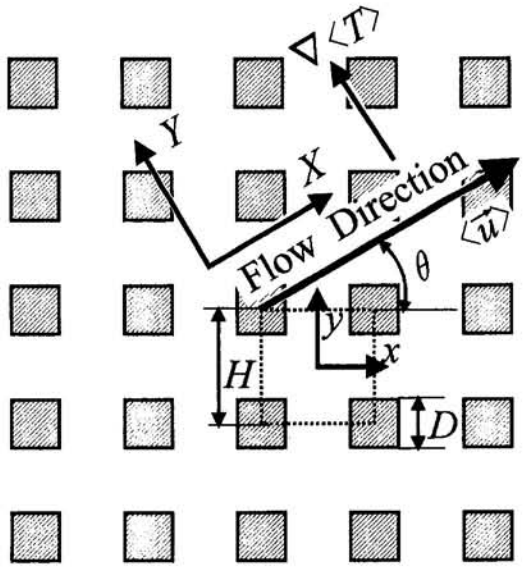

Fig. 1 Numerical model and its coordinates

$$\langle \vec{u} \rangle = |\langle \vec{u} \rangle|(\cos\theta \vec{i} + \sin\theta \vec{j}) \quad (1)$$

$$\nabla\langle T \rangle = \frac{\Delta T}{H}(-\sin\theta \vec{i} + \cos\theta \vec{j}) \quad (2)$$

where $\langle\ \rangle$ denotes volume average, namely,

$$\langle \phi \rangle = \frac{1}{V}\int_V \phi dV$$

The control volume V is much smaller than a macroscopic characteristic length and can be taken as H^2 for this periodic structure. Due to the periodicity of the model, only one structural unit as indicated by dashed lines may be taken as a calculation domain. The governing equations for the whole domain (i.e., fluid and solid phases) are given as follows:

$$\nabla \cdot \vec{u} = 0 \quad (3)$$

$$(\nabla \cdot \vec{u})\vec{u} = -\frac{1}{\rho}\nabla p + \nu\nabla^2\vec{u} \quad (4)$$

$$\rho_f C_{p_f} \nabla \cdot (\vec{u}T) = k_f \nabla^2 T: \quad \text{fluid phase} \quad (5)$$

$$k_s \nabla^2 T = 0: \quad \text{solid phase} \quad (6)$$

where the subscripts f and s denote fluid and solid phases, respectively. The boundary, compatibility, and periodic constraints are given by:

On the solid walls:

$$\vec{u} = \vec{0} \quad (7)$$

$$T_s = T_f \quad (8a)$$

$$k_s \left.\frac{\partial T}{\partial n}\right|_s = k_f \left.\frac{\partial T}{\partial n}\right|_f \quad (8b)$$

On the periodic boundaries:

$$\vec{u}|_{x=-H/2} = \vec{u}|_{x=H/2} \quad (9a)$$

$$\vec{u}|_{y=-H/2} = \vec{u}|_{y=H/2} \quad (9b)$$

$$\int_{-H/2}^{H/2} u dy\Big|_{x=-H/2} = \int_{-H/2}^{H/2} u dy\Big|_{x=H/2} = H|\langle \vec{u} \rangle| \cos\theta \quad (10a)$$

$$\int_{-H/2}^{H/2} v dx\Big|_{y=-H/2} = \int_{-H/2}^{H/2} v dx\Big|_{y=H/2} = H|\langle \vec{u} \rangle| \sin\theta \quad (10b)$$

$$T|_{x=-H/2} = T|_{x=H/2} + \Delta T \sin\theta \quad (11a)$$

$$T|_{y=-H/2} = T|_{y=H/2} - \Delta T \cos\theta \quad (11b)$$

We shall define the Reynolds number based on the Darcian velocity $|\langle \vec{u} \rangle|$ and length of structural unit H as $\mathrm{Re} = |\langle \vec{u} \rangle| H/\nu$.

Method of Computation

The governing equations are discretized by integrating them over a grid volume. The SIMPLE algorithm for the pressure-velocity coupling, as proposed by Patankar and Spalding (1972), is adopted to correct the pressure and velocity fields. Calculation starts with solving the two momentum equations, and subsequently, the estimated velocity field is corrected by solving the pressure correction equation reformulated from the discretized continuity and momentum equations, such that the velocity field fulfills the continuity principle. Then, the energy conservation equation is solved to find the corresponding temperature field. This iteration sequence is repeated until convergence is achieved. Convergence is measured in terms of the maximum change in each variable during an iteration. The maximum change allowed for the convergence check is set to 10^{-5}, as the variables are normalized by appropriate references. A fully implicit scheme is adopted with the hybrid differencing scheme for the advection terms. Further details on this numerical procedure can be found from Patankar (1980) and Nakayama (1995).

Nomenclature

$\vec{A}$ = surface area vector
A_{int} = total interface between the fluid and solid
b = Forchheimer constant
C_p = specific heat at constant pressure
C_s = specific heat of solid
D = size of square rod
H = size of structural unit
$\vec{i}, \vec{j}$ = unit vectors in the x and y directions
k = thermal conductivity
K = permeability
p = microscopic pressure
Pe = Peclet number based on H and the macroscopically uniform velocity
Re = Reynolds number based on H and the macroscopically uniform velocity
T = microscopic temperature
$\langle T'\vec{u}' \rangle$ = dispersion vector
ΔT = macroscopic temperature difference across a structural unit
u, v = microscopic velocity components in the x and y directions
V = control volume
x, y = Cartesian coordinates
X, Y = coordinates set along the macroscopic flow direction and its normal
ϵ = porosity
θ = macroscopic flow angle
ν = kinematic viscosity
ρ = density

Subscripts and Superscripts

dis = dispersion
e = effective
f = fluid
s = solid
tor = tortuosity

Special Symbols

$\langle\ \rangle$ = volume average
$\langle\ \rangle^{f,s}$ = intrinsic average

All computations have been carried out for a one structural unit $H \times H$ using nonuniform grid arrangements with 45×45. Sample calculations were also carried out using a finer grid system, 80×80, to ensure that the results are independent of the grid system. The Reynolds number was varied from 10^{-2} to 10^3 (assuming a typical range of $H = 1$ mm $\sim$ 1 cm); the ratio of the solid phase thermal conductivity to the fluid phase k_s/k_f, from 2 to 100; and the porosity ϵ, from 0.1 to 0.96, whereas the Prandtl number was fixed at 0.71. All computations were performed using the computer system CONVEX 220 at Shizuoka University Computer Center.

Volume-Averaged Energy Equation and Expressions for Tortuosity and Thermal Dispersion

Following Cheng (1978) and Nakayama (1995), we integrate the microscopic energy equation, Eq. (5), for the incompressible fluid over an elementary control, and obtain

$$\rho_f C_{p_f}\left[\frac{\partial \epsilon\langle T\rangle^f}{\partial t} + \langle \vec{u}\rangle \cdot \nabla\langle T\rangle^f\right] = \nabla \cdot \left[k_f \nabla \epsilon\langle T\rangle^f + \frac{1}{V}\int_{A_{\text{int}}} k_f T d\vec{A} - \rho_f C_{p_f}\langle T'\vec{u}'\rangle\right] + \frac{1}{V}\int_{A_{\text{int}}} k_f \nabla T \cdot d\vec{A} \quad (12)$$

Similarly, the microscopic energy equation for the solid, Eq. (6), may be integrated to give

$$\rho_s C_s \frac{\partial (1-\epsilon)\langle T\rangle^s}{\partial t} = \nabla \cdot \left[k_s \nabla (1-\epsilon)\langle T\rangle^s - \frac{1}{V}\int_{A_{\text{int}}} k_s T d\vec{A}\right] - \frac{1}{V}\int_{A_{\text{int}}} k_f \nabla T \cdot d\vec{A} \quad (13)$$

where A_{int} is the total interface between the fluid and solid, while $d\vec{A}$ is its vector element pointing outward from the fluid side to solid side. $\langle T\rangle^f$ and $\langle T\rangle^s$ are the intrinsic average of the fluid temperature and that of the solid phase, respectively. The continuity of heat flux at the interface is implemented in Eq. (13). We shall assume that thermal equilibrium exists between the fluid and solid matrix, namely, $\langle T\rangle^f = \langle T\rangle^s = \langle T\rangle$. For the present case of steady periodic flow, the thermal equilibrium condition proves to be exact. Adding up Eqs. (12) and (13), we have

$$[\epsilon \rho_f C_{p_f} + (1-\epsilon)\rho_s C_s]\frac{\partial \langle T\rangle}{\partial t} + \rho_f C_{p_f}\langle \vec{u}\rangle \cdot \nabla\langle T\rangle = \nabla \cdot \left\{[\epsilon k_f + (1-\epsilon)k_s]\nabla\langle T\rangle + \frac{1}{V}\int_{A_{\text{int}}} (k_f - k_s) T d\vec{A} - \rho_f C_{p_f}\langle T'\vec{u}'\rangle\right\} \quad (14)$$

For the case of steady flow, we rewrite Eq. (14) as

$$\rho_f C_{p_f}\langle \vec{u}\rangle \cdot \nabla\langle T\rangle = \nabla \cdot \{(k_e \bar{\bar{I}} + \bar{\bar{k}}_{\text{tor}} + \bar{\bar{k}}_{\text{dis}}) \cdot \nabla\langle T\rangle\} \quad (15)$$

where

$$k_e \equiv \epsilon k_f + (1-\epsilon)k_s \quad (16)$$

$$\frac{1}{V}\int_{A_{\text{int}}} (k_f - k_s) T d\vec{A} \equiv \bar{\bar{k}}_{\text{tor}} \cdot \nabla\langle T\rangle \quad (17)$$

$$-\rho_f C_{p_f}\langle T'\vec{u}'\rangle \equiv \bar{\bar{k}}_{\text{dis}} \cdot \nabla\langle T\rangle \quad (18)$$

The first two terms $-(k_e \bar{\bar{I}} + \bar{\bar{k}}_{\text{tor}}) \cdot \nabla\langle T\rangle$ on the right-hand side of Eq. (15) account for the molecular diffusion, whereas the third term $-\bar{\bar{k}}_{\text{dis}} \cdot \nabla\langle T\rangle$ accounts for contributions from thermal (mechanical) dispersion. k_e defined in Eq. (16) is the stagnant thermal conductivity. The apparent conductivity tensors $\bar{\bar{k}}_{\text{tor}}$ and $\bar{\bar{k}}_{\text{dis}}$ are introduced to model the tortuosity molecular diffusion term and the thermal dispersion term, respectively, by a gradient-type diffusion hypothesis. For the case of low-Peclet-number flow with the assumption of equal fluid and solid conductivities (Koch et al., 1989), both the tortuosity and dispersion terms may be dropped, and we have

$$\rho_f C_{p_f}\langle \vec{u}\rangle \cdot \nabla\langle T\rangle = \nabla \cdot (k_e \nabla\langle T\rangle) \quad (19)$$

In contrast, for the case of high-Peclet-number flow, the thermal dispersion predominates over the molecular diffusion such that

$$\rho_f C_{p_f}\langle \vec{u}\rangle \cdot \nabla\langle T\rangle = \nabla \cdot (\bar{\bar{k}}_{\text{dis}} \cdot \nabla\langle T\rangle) \quad (20)$$

For the case of high-Peclet-number flow, differences in the stagnant conductivity no longer affect macroscopic heat transfer in porous media. In this study, we shall determine both the tortuosity and thermal dispersion conductivities purely from a theoretical basis by substituting the microscopic numerical results into Eqs. (17) and (18).

When one coordinate is set along the macroscopic flow direction, only diagonal components of the tortuosity and dispersion conductivity tensors remain nonzero. Since the macroscopically linear temperature gradient is imposed along the Y direction normal to the X direction of macroscopic flow in the present model, the YY components of $\bar{\bar{k}}_{\text{tor}}$ and $\bar{\bar{k}}_{\text{dis}}$ can readily be determined from

$$(k_{\text{tor}})_{YY} = \frac{\left(\frac{k_s - k_f}{V}\int_{A_{\text{int}}} T d\vec{A}\right) \cdot (-\sin\theta \vec{i} + \cos\theta \vec{j})}{(\Delta T/H)} \quad (21)$$

$$(k_{\text{dis}})_{YY} = \frac{-\frac{\rho_f C_{p_f}}{H^2}}{(\Delta T/H)}\int_{-H/2}^{H/2}\int_{-H/2}^{H/2} (T - \langle T\rangle)(\vec{u} - \langle \vec{u}\rangle^f) dx dy \times (-\sin\theta \vec{i} + \cos\theta \vec{j}) \quad (22)$$

respectively.

Results and Discussion

Microscopic Velocity Field and Macroscopic Pressure Gradient. Two distinct velocity vector plots obtained at $\theta = 0$ and 45 deg for three different Reynolds numbers, namely, Re $= 10^{-1}$, 10, and 10^3, are compared in Fig. 2. When the Reynolds number is comparatively small, say Re $\leq$ 10, the velocity profiles for both $\theta = 0$ and 45 deg exhibit parabolic profiles as in a fully developed channel flow such that the viscous force contribution to the pressure drop predominates over the inertial contribution. As the Reynolds number increases, a distinct difference appears between the velocity field of $\theta = 0$ deg and that of $\theta = 45$ deg. Flow separation takes place for $\theta = 45$ deg, such that the inertial contribution to the pressure drop becomes significant, whereas the flow field for $\theta = 0$ deg remains of the channel flow type such that the inertial contribution is negligibly small. Accordingly, we may expect that the resulting macroscopic pressure drop for a fixed mass flow rate would be fairly insensitive to the macroscopic flow direction for low-Reynolds-number flows, while it becomes sensitive to the flow direction as the Reynolds number grows high.

The macroscopic pressure gradient (i.e., the gradient of the intrinsic average pressure measured along the macroscopic flow direction) of our primary interest may readily be evaluated using the microscopic numerical results as

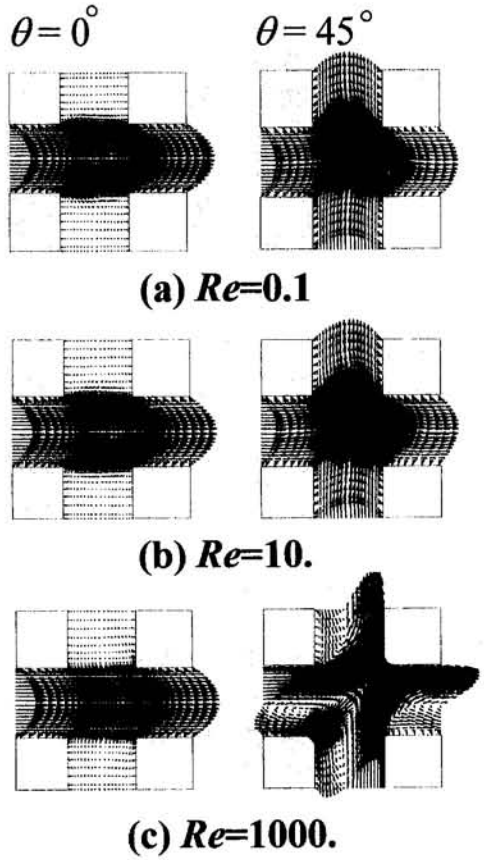

Fig. 2 Velocity vector plots

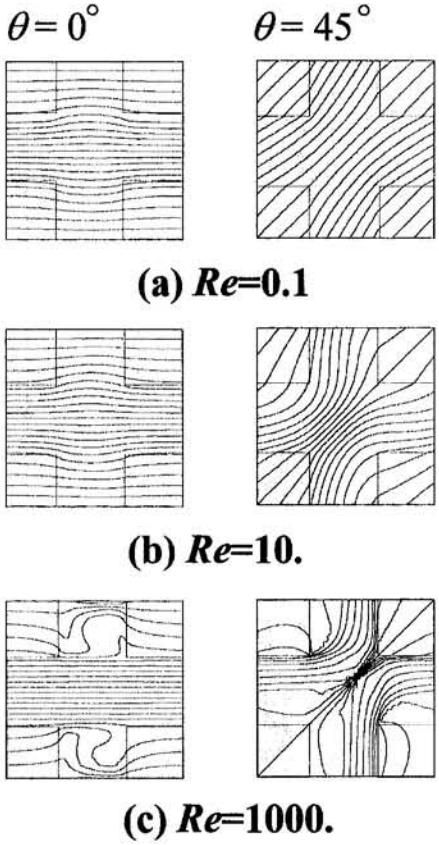

Fig. 4 Isotherms

$$-\frac{d\langle p\rangle^f}{dX} = \frac{\cos\theta}{H(H-D)}\int_{-(H-D)/2}^{(H-D)/2}(p|_{x=-(H-D)/2} - p|_{x=(H-D)/2})dy + \frac{\sin\theta}{H(H-D)} \times \int_{-(H-D)/2}^{(H-D)/2}(p|_{y=-(H-D)/2} - p|_{y=(H-D)/2})dx \quad (23)$$

The pressure gradient results, thus obtained with $\epsilon = 0.64$, changing the Reynolds number and macroscopic flow angle are assembled in Fig. 3, in terms of the dimensionless pressure gradient against the Reynolds number. All data show that the dimensionless pressure gradient stays constant for Re $\leq$ 10, irrespective of the flow angle, as we expected from the velocity vector plots in Fig. 2. The pressure gradient increases drastically as Re goes beyond 10 in which the porous inertial contribution becomes appreciable as compared with the viscous (Darcian) contribution.

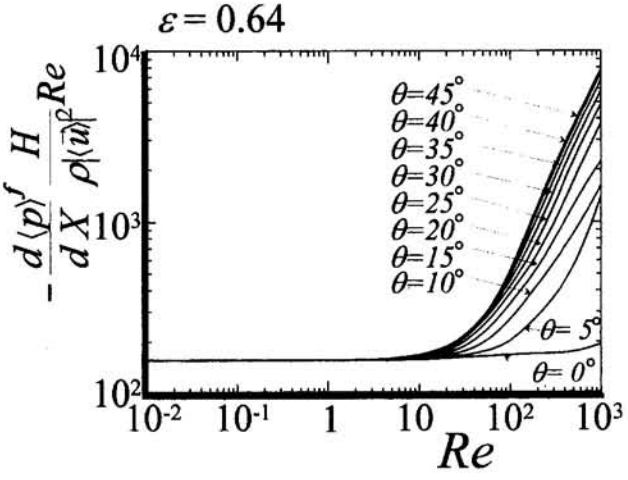

Fig. 3 Dimensionless pressure gradient

The Forchheimer–extended Darcy law may be written as

$$-\frac{d\langle p\rangle^f}{dX}\frac{H}{\rho|\langle\vec{u}\rangle|^2}\,\mathrm{Re} = \frac{H^2}{K} + bH\,\mathrm{Re} \quad (24)$$

Thus, the permeability K may readily be determined by reading the intercept of the ordinate variable in Fig. 3. The constancy of the dimensionless pressure gradient, irrespective of θ, substantiates the validity of the periodic numerical models to determine K from the first principles. The second term on the right-hand side of Eq. (24) represents the porous inertial contribution, which increases with Re. The coefficient b for the inertial contribution may be determined by fitting the numerical results obtained at high Reynolds numbers into Eq. (24). Such an attempt and its extension to a three-dimensional model have been recently reported by Nakayama et al. (1995).

Microscopic Temperature Field and Thermal Conductivity Due to Tortuosity. The microscopic temperature fields obtained at $\theta = 0$ and 45 deg with $\epsilon = 0.64$ are shown for Re = 10^{-1}, 10, and 10^3 in Fig. 4 in terms of isotherms. The isotherms obtained at low Reynolds numbers exhibit a typical pattern for the case of pure thermal conduction. For the case of high-Reynolds-number flows, the temperature pattern becomes very complex, as a result of thermal dispersion, as seen from Fig. 4(*c*), where comparatively uniform temperature regions exist

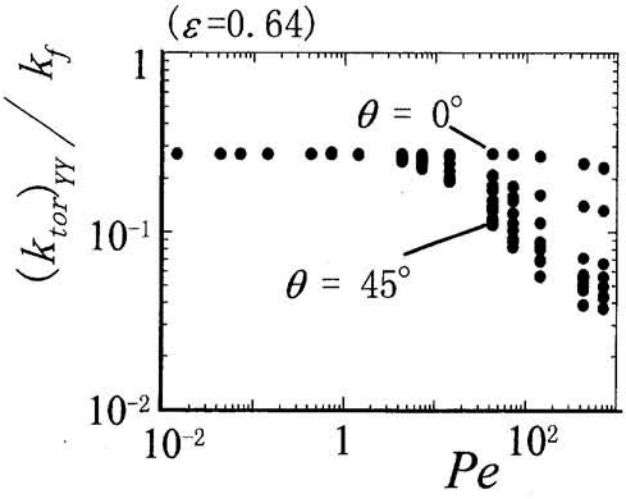

Fig. 5 Apparent thermal conductivity due to tortuosity

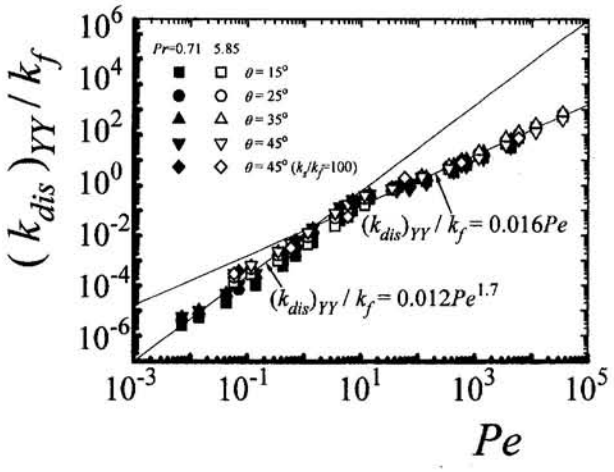

Fig. 7 Apparent thermal conductivity due to dispersion

within recirculation regions. In Fig. 5, the tortuosity conductivity $(k_{tor})_{YY}$ determined by feeding the microscopic numerical results into Eq. (21) is plotted against the Peclet number Pe for the case of $\epsilon = 0.64$. It is interesting to note that all data obtained for different macroscopic flow angles fall onto a horizontal asymptote as Pe decreases. An approximate analytical formula for this asymptotic value may be found by approximating the temperature distribution in a structural unit at low Peclet number (see Fig. 4(*a*)) by a piecewise linear temperature distribution within a one-dimensional composite slab, as

$$\frac{(k_{tor})_{YY}}{k_f} = \left(\frac{k_s}{k_f} - 1\right) \frac{(1-\epsilon)}{(1-\epsilon)^{1/2} + \frac{k_s}{k_f}(1-(1-\epsilon)^{1/2})} \quad (25)$$

The tortuosity conductivity results obtained for a low-Peclet-number range as the porosity is changed from 0.1 to 0.96, and thermal conductivity ratio from 2 to 100, are plotted with the curves generated by the foregoing approximate formula in Fig. 6 with the abscissa $(1 - \epsilon)$. An excellent agreement can be seen between the numerical results and the approximate formula for the entire range of porosity.

Figure 5 clearly shows that the tortuosity conductivity decreases as Pe increases. However, the contribution from thermal dispersion predominates over the tortuosity contribution as Pe increases, such that the tortuosity conductivity may no longer be important and may well be neglected in such a high-Peclet-number range.

Thermal Conductivity Due to Thermal Dispersion. The microscopic temperature results obtained for 15 deg $\leq \theta \leq$ 45 deg with Pr = 0.71, 5.85, and k_s/k_f = 2, 100, are processed using Eq. (22), and the resulting thermal conductivity $(k_{dis})_{YY}$ due to thermal dispersion is plotted for the case of $\epsilon = 0.64$ in Fig. 7. The figure suggests that the lower and higher Peclet number data follow two distinct limiting lines, respectively. The lower Peclet number data vary in proportion to $Pe^{1.7}$, whereas the high-Peclet-number data vary in proportion to Pe. The Peclet number dependency at low Pe, namely, $Pe^{1.7}$, which is the same as what Eidsath et al. (1983) observed numerically for the axial thermal dispersion conductivity, but different from Pe^2 suggested by Taylor (1953) and Aris (1956) in the classical study of solute in a fluid flowing in a tube. A further analytical and numerical investigation is needed to clarify this difference in the Peclet number dependency at low Pe. Exhaustive computations were conducted to extract functional relationships for the thermal dispersion conductivities at low and high Peclet number ranges, $0.01 < Pe < 10$ and $10 < Pe < 5000$, respectively. The thermal dispersion conductivities obtained for different ϵ are plotted in Fig. 8 with the abscissa variable $(1 - \epsilon)$ to investigate the porosity dependency. The resulting expressions for the low and high Peclet number ranges are given by

$$\frac{(k_{dis})_{YY}}{k_f} = 0.022 \frac{Pe_D^{1.7}}{(1-\epsilon)^{1/4}} \quad \text{for} \quad (Pe_D < 10) \quad (26a)$$

$$\frac{(k_{dis})_{YY}}{k_f} = 0.052(1-\epsilon)^{1/2} Pe_D \quad \text{for} \quad (Pe_D > 10) \quad (26b)$$

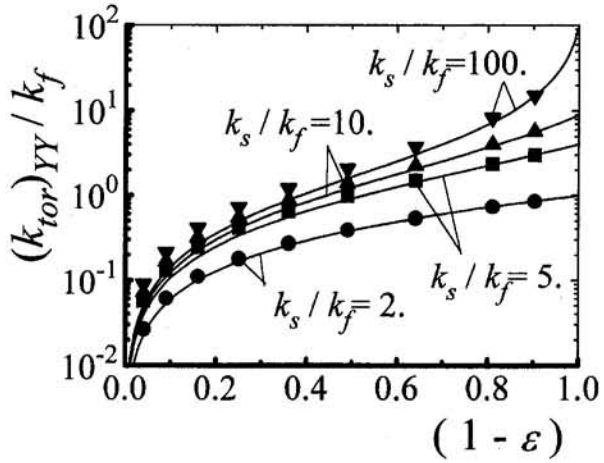

Fig. 6 Apparent thermal conductivity due to tortuosity as a function of porosity

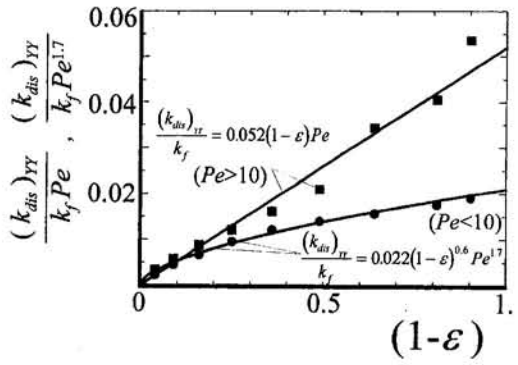

Fig. 8 Apparent thermal conductivity due to dispersion as a function of porosity

where the relationship $Pe_D = Pe(1 - \epsilon)^{1/2}$ is used.

The predicted total thermal conductivity $(k_e + (k_{tor})_{YY} + (k_{dis})_{YY})$ is compared against the experimental data of Fried and Combarnous (1971), Han et al. (1985), and Yagi et al. (1960) for packed beds in Fig. 9, where a fairly good agreement can be seen between the present correlation and the experimental data, in light of the simplicity of the present periodic model. In the same figure, Koch and Brady's (1985) Stokes flow analysis on dilute suspension of particles is shown for reference. Their analysis, however, should be compared with the experimental data with caution, since their analysis applies only for the case of high porosity, and their leading order analysis of Stokes flow of high-Prandtl-number fluid takes no account of the Reynolds number effects, which are definitely included in Fried and Combarnous' experimental data.

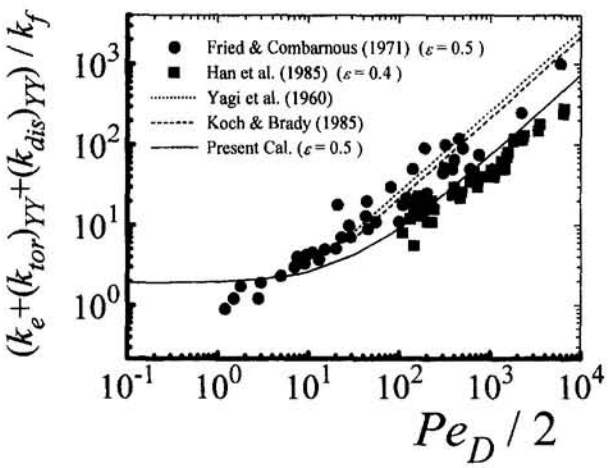

Fig. 9 Comparison of the prediction and experiment

Concluding Remarks

A successful attempt was made to investigate the apparent conductivities due to the tortuosity and thermal dispersion numerically, considering a macroscopically uniform flow through a periodic model of square rods. The transverse components of the conductivities were determined imposing a macroscopically linear temperature gradient normal to the macroscopic flow direction. The corresponding streamwise components of the conductivities may be determined similarly, by imposing a temperature gradient parallel to the flow direction. Such an attempt is under way.

Acknowledgments

One author (A.N.) wishes to thank Dr. E. Arquis for kindly sending copies of his papers and for the inspiring discussion held at Brighton in the summer of 1994.

References

Aris, R., 1956, "On the Dispersion of a Solute in a Fluid Flowing Through a Tube," *Proc. Roy. Soc. London,* Vol. A235, pp. 67–77.

Arquis, E., Caltagirone, J. P., and Le Breton, P., 1991, "Détermination des propriétés de dispersion d'un milieu périodique à partir de l'analyse locale des transferts," *C.R. Acad. Sci. Paris,* Vol. II, No. 313, pp. 1087–1092.

Arquis, E., Caltagirone, J. P., and Delmas, A., 1993, "Derivation in Thermal Conductivity of Porous Media Due to High Interstitial Flow Velocity," *Proc. 22nd Int. Thermal Conductivity Conf.,* Tempe, AZ, Nov.

Cheng, P., 1978, "Heat Transfer in Geothermal Systems," *Advances in Heat Transfer,* Vol. 14, pp. 1–105.

Coulaud, O., Morel, P., and Caltagirone, J. P., 1988, "Numerical Modeling of Nonlinear Effects in Laminar Flow Through a Porous Medium," *J. Fluid Mech.,* Vol. 190, pp. 393–407.

Edwards, D. A., Shapiro, M., Brenner, H., and Shapira, M., 1991, "Dispersion of Inert Solutes in Spatially Periodic Two-Dimensional Model Porous Media," *Transport in Porous Media,* Vol. 6, pp. 337–358.

Eidsath, A., Carbonell, R. G., Whitaker, S., and Herman, L. R., 1983, "Dispersion in Pulsed Systems: III. Comparison Between Theory and Experiment for Packed Beds," *Chem. Engng. Sci.,* Vol. 38, pp. 1803–1816.

Fowler, A. J., and Bejan, A., 1994, "Forced Convection in Banks of Inclined Cylinders at Low Reynolds Numbers," *Int. J. Heat Fluid Flow,* Vol. 15, pp. 90–99.

Fried, J. J., and Combarnous, M. A., 1971, "Dispersion in Porous Media," *Advances in Hydro. Science,* Vol. 7, pp. 169–282.

Han, N.-W., Bhakta, J., and Carbonell, R. G., 1985, "Longitudinal and Lateral Dispersion in Packed Beds: Effect of Column Length and Particle Size Distribution," *AIChE J.,* Vol. 31, pp. 277–288.

Katsuki, S., and Nakayama, A., 1990, *Numerical Simulation of Heat and Fluid Flow,* Morikita Shuppan, Tokyo.

Kawamura, Y., 1994, "Numerical Simulation of Microscopic Flow in a Porous Structure," M.S. Thesis, Shizuoka University, Japan.

Koch, D. L., and Brady, J. F., 1985, "Dispersion in Fixed Beds," *J. Fluid Mech.,* Vol. 154, pp. 399–427.

Koch, D. L., Cox, R. G., Brenner, H., and Brady, J. F., 1989, "The Effect of Order on Dispersion in Porous Media," *J. Fluid Mech.,* Vol. 200, pp. 173–188.

Kuwahara, F., Nakayama, A., and Koyama, H., 1994, "Numerical Modelling of Heat and Fluid Flow in a Porous Medium," *Proc. 10th Int. Heat Transfer Conf.,* Vol. 5, pp. 309–314.

Larson, R. E., and Higdon, J. J. L., 1989, "A Periodic Grain Consolidation Model of Porous Media," *Physics of Fluids,* Vol. A1, pp. 38–46.

Nakayama, A., 1995, *PC-Aided Numerical Heat Transfer and Convective Flow,* CRC Press, Boca Raton, FL.

Nakayama, A., Kuwahara, F., Kawamura, Y., and Koyama, H., 1995, "Three-Dimensional Numerical Simulation of Flow Through a Microscopic Porous Structure," *Proc. ASME/JSME Thermal Engineering Conf.,* Vol. 3, pp. 313–318.

Patankar, S. V., and Spalding, D. B., 1972, "A Calculation Procedure for Heat, Mass and Momentum Transfer in Three-Dimensional Parabolic Flows," *Int. J. Heat Mass Transfer,* Vol. 15, pp. 1787–1806.

Patankar, S. V., 1980, *Numerical Heat Transfer and Fluid Flow,* Hemisphere, Washington, DC.

Quintard, M., and Whitaker, S., 1993, "One- and Two-Equation Models for Transient Diffusion Processes in Two-Phase Systems," *Advances in Heat Transfer,* Vol. 23, pp. 369–464.

Sahraoui, M., and Kaviany, M., 1991, "Slip and No-Slip Boundary Condition at Interface of Porous, Plain Media," *Proc. ASME/JSME Thermal Engineering Proceedings,* Vol. 4, pp. 273–286.

Taylor, G. I., 1953, "Dispersion of Solute Matter in Solvent Flowing Slowly Through a Tube," *Proc. Roy. Soc. London,* Vol. A219, pp. 186–203.

Yagi, S., Kunii, D., and Wakao, N., 1960, "Studies on Axial Effective Thermal Conductivities in Packed Beds," *AIChE J.,* Vol. 6, pp. 543–546.